ACS OMEGA

Open Access

http://pubs.acs.org/journal/acsodf

Article

Experimental Study on the Effect of Wetting−Drying Cycles on Crack Development and Radon Retardation of the Covering Soil in Uranium Mill Tailing Impoundments

Zhanyuan Zhang, Changshou Hong,* Xiangyang Li, and Hong Wang

Cite This: *ACS Omega* 2024, 9, 19295−19310

Read Online

ACCESS | Metrics & More | Article Recommendations

ABSTRACT: The majority of uranium mill tailing impoundments in the southern part of China are located in humid subtropical regions where persistent rainfall and rapid evaporation of water after rain often occur. Under the prolonged influence of alternating wet and dry conditions, the covering soil layer of uranium mill tailing impoundments develops cracks, leading to the issue of degradation or even failure of the radon retardation effect. A beach surface of uranium mill tailing impoundments in the southern part of China is selected as the research object. Through use of a self-made simulation test device, a degradation experiment of uranium mill tailing covering soil models under wetting−drying cycles was conducted indoors. The experimental results indicate that with a constant amplitude of wetting−drying cycles, microcracks characterized by a narrow width and high abundance were mainly generated in the early-to-mid-stage of wetting−drying cycles. The main cracks, characterized by their wide width and less abundance, were mainly formed in the mid-to-late stage of wetting−drying cycles. After seven wetting−drying cycles, the total length of cracks showed a "stair-step" increase and the surface crack ratio exhibited a trend of moving from rapid growth to stable growth and then to a slight decline. The cumulative damage degree showed a rapid increase to stable growth with an increase in the number of wetting−drying cycles. Grey relational analysis revealed that, compared to other surface crack indicators, radon exhalation rate was the most closely correlated with the surface crack ratio. With a constant amplitude of wetting−drying cycles, the radon exhalation rate underwent four stages as the number of wetting−drying cycles increased: stage I witnessed a rapid increase, stage II witnessed a rapid decrease, stage III witnessed a gradual increase, and stage IV witnessed a stable or even slight decrease. With a constant number of wetting−drying cycles, the radon exhalation rate correspondingly increased with the amplitude of wetting−drying cycles, particularly noticeable when the alternation amplitude was 30 ± 20%. From the early mid-stage to the late stage of wetting−drying cycles, the curves of the radon exhalation rate, surface crack ratio, and cumulative damage degree tended to be consistent, showing a gradual increase. The research provided in this study offers valuable insights into radon control measures and environmental assessments on the beach surface of uranium mill tailing impoundments.

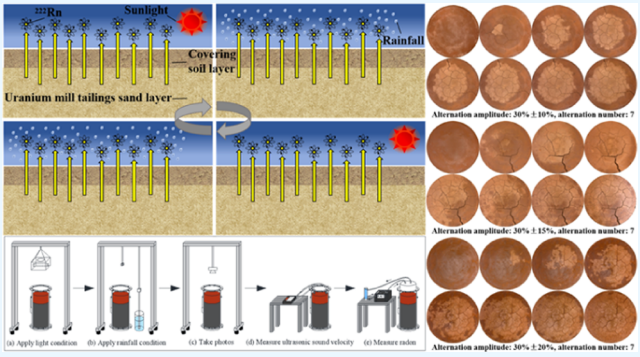

1. INTRODUCTION

Nuclear energy, as an economical and scalable clean energy source, plays a significant role in replacing traditional energy and promoting ecological civilization, making it an indispensable part of China's new energy strategy. With the development and utilization of nuclear energy, China's nuclear power industry has seen rapid growth, leading to an increasing demand for natural uranium. During uranium mining and hydrometallurgical processes, a large number of uranium tailings are generated. Uranium mill tailings represent a long-term potential source of radioactive pollution, containing many radionuclides such as ^{238}U, ^{234}U, ^{230}Th, ^{226}Ra, ^{222}Rn, ^{210}Po, and ^{210}Pb, which constitute 70−85% of the total radioactivity of original ores.[1] Radon (^{222}Rn) emitted from the beach surface of uranium mill tailing impoundments accounts for approximately 25% of the collective dose to the surrounding public in the entire uranium mining and metallurgy system, posing a potential hazard to the public and the environment around uranium mill tailing impoundments. Radon and its progeny enter the human body through respiration, ingestion, and other ways, causing internal exposure. Prolonged inhalation of high

Received: January 11, 2024
Revised: April 9, 2024
Accepted: April 10, 2024
Published: April 18, 2024

concentrations of radon can lead to damage to the upper respiratory tract and lungs of humans, even resulting in lung cancer.[2] According to Regulations for Radiation Protection and Radiation Environment Protection in Uranium Mining and Milling, after decommissioning and environmental remediation of uranium mill tailing impoundments, the retirement management limit for the surface radon exhalation rate should not exceed 0.74 Bq/(m^2·s). However, the average radon exhalation rate on the beach surface of uranium mill tailing impoundments in China is approximately 3.25−9.85 Bq/(m^2·s), significantly exceeding the retirement management limit. Therefore, safe decommissioning and remediation of uranium mill tailing impoundments have been prioritized as a key task in radiation protection and environmental protection in China.

Since the 21st century, extreme climate change has become a globally recognized focal point. Numerous uranium mill tailing impoundments in the southern part of China are located in regions with a humid subtropical climate, where recurrent weather phenomena such as prolonged high temperature and persistent rainfall are prevalent. These conditions directly impact the spatiotemporal distribution of evaporation and precipitation, leading to repeated wetting−drying cycles of the soil.[3] During the alternating drying and wetting phases, physical and mechanical properties of the covering soil in uranium mill tailing impoundments undergo significant changes, resulting in the phenomena of swelling and shrinking. This affects the distribution of soil pores, leading to alterations in the soil volume and crack development, thereby influencing the stability of the soil structure.[4] Additionally, continuous radioactive decay within uranium mill tailings releases a constant stream of heat, subjecting the beach surface cover system of uranium mill tailing impoundments to a prolonged thermal load. This further accelerates the evaporation of moisture in the cover soil layer. Consequently, initiation and development of cracks provide advantageous channels for radon to diffuse into the atmosphere, which leads to the gradual degradation and even failure of the radon retardation effect of the covering soil in uranium mill tailing impoundments, exerting a negative impact on the long-term stability of uranium mill tailing impoundments.

Currently, covering the disposal remains the most commonly used method for mitigating radon exhalation in the management of uranium mill tailing impoundment beach surfaces, which can be categorized into single-layer covering and multilayer covering.[5] Single-layer covering primarily focuses on the effectiveness of radon shielding. Domestic and international scholars have conducted extensive research on this topic. Leoni et al.[6] and Ferry et al.[7] suggested the use of stable, low-permeability, and low-radioactivity materials such as soil to cover uranium mill tailings for reducing radon release into the atmosphere. Regarding the effect of different types of covering materials[8−10] and related physical properties such as thickness,[11−13] density,[14] compaction,[15,16] moisture content,[17,18] porosity,[19,20] particle size fractal,[21,22] and permeability[23] on anomalous radon exhalation from the beach surface of uranium mill tailing impoundments, Tan et al.[9] studied the effectiveness of different coverings in reducing radon exhalation from uranium mill tailings and found that red soil had the best radon reduction effect. Regarding the effect of internal and external forces[24−30] on anomalous radon exhalation from the beach surface of uranium mill tailing impoundments, Li et al.[30] analyzed and demonstrated the possibility of hydraulic erosion, wind erosion, and freeze−thaw erosion on the covering layer of a decommissioned uranium mill tailing impoundment. In the case of multilayer covering, the beach surface cover system of uranium mill tailing impoundments typically includes a soil-vegetation layer, a sand-gravel drainage layer, and a compacted clay layer from the top to the bottom.[31−33] This system not only effectively reduces the radon exhalation rate but also enhances the erosion resistance and impermeability. Xin et al.[33] reviewed the research progress of the uranium mill tailing treatment technology including covering treatment, solidification treatment, backfill treatment, and bioremediation. In summary, many scholars have extensively studied the effect of the physical properties of covering materials on the radon exhalation rate on the beach surface of uranium mill tailing impoundments. This study correlates the variation in the radon exhalation rate on the covering soil of uranium mill tailing impoundments with the development of surface cracks (number of cracks, total length of cracks, average width of cracks, and surface crack rate) and the cumulative of internal damage under wetting−drying cycles. By using surface crack indicators and the cumulative damage degree, we further investigate the effect of wetting−drying cycles on the radon retardation of the covering soil in uranium mill tailings.

In southern China, red soil is commonly chosen as the covering material based on the principle of adapting to local conditions and using local resources.[34] Existing data indicates that some beach surface cover systems of uranium mill tailing impoundments in southern China suffered severe erosion and damage, which directly threatened the bottom layer (soil layer) and even revealed exposed uranium mill tailings. The formation of cracks in the compacted soil layer is the fundamental reason for the degradation of the radon retardation effect. When studying the radon shielding effect of the covering soil layer of uranium tailings, the development of surface cracks of the covering soil layer should be fully considered. Observation methods for soil crack evolution include the ultrasonic method, resistivity method, computer tomography method, scanning electron microscopy method, digital image method, remote optical microscopy method, and so on. Crack parameters can be used as quantitative indicators to describe the degree of crack evolution. However, issues such as test conditions and cost limit the promotion of some methods. The digital image method has the advantages of being fast, accurate, and low-cost. It is currently a commonly used method for continuously observing soil cracks nondestructively. It has been widely adopted by scholars and has yielded fruitful research results.[35−39] Duan et al.[36] quantitatively studied the soil crack characteristics of the plowed layer and the subsoil layer in rice paddies using the digital image processing method and obtained the development law of soil cracks under alternating dry and wet conditions. Chen[38] used the computer image processing technology and the triaxial test to analyze the evolution law of red clay cracks and the variation law of shear strength indicators under drying−wetting cycles. He established the relationship between the shear strength indicators of red clay and crack density. The initiation, development, and expansion of cracks on the covering soil of uranium mill tailing impoundments during wetting−drying cycles inevitably affect the efficiency of radon reduction in the covering soil. Therefore, there is an urgent need to systematically conduct indoor experiments on the degradation of the uranium mill tailing covering soil models under wetting−drying cycles. This research aims to explore the effect

https://doi.org/10.1021/acsomega.4c00374
ACS Omega 2024, 9, 19295−19310

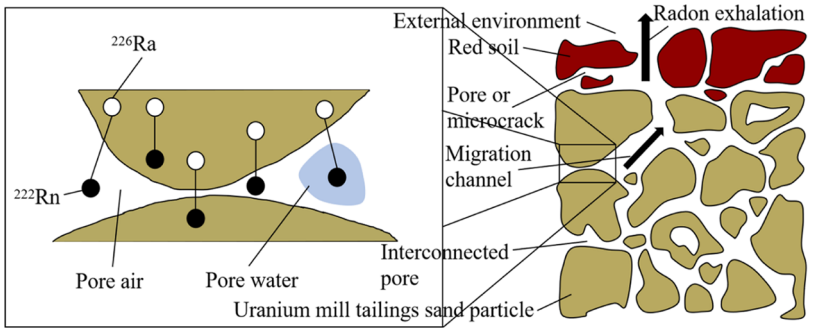

Figure 1. Radon exhalation process on the surface of the uranium mill tailing covering soil.

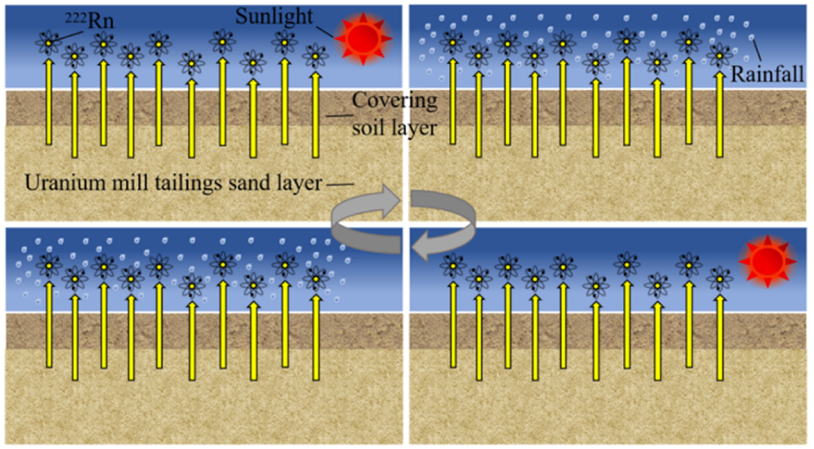

Figure 2. Radon exhalation model of the uranium mill tailing covering soil under wetting−drying cycles.

of wetting−drying cycles on crack development and the radon retardation of the covering soil in uranium mill tailing impoundments, which can provide a theoretical basis for assessing the safety and the stability of beach surface cover systems of uranium mill tailing impoundments.

2. EXPERIMENTAL SECTION

2.1. Radon Migration Pattern in the Covering Soil Layer of Uranium Mill Tailing Impoundments. A large amount of radioactive material is stored in uranium mill tailing impoundments. Radium decays into radon. Radon diffuses from the uranium mill tailing sand layer to the red soil layer and then releases into the external environment. The entire process is divided into three stages, as illustrated in Figure 1.

The first stage is generation of radon. Radium atoms within solid lattices of uranium mill tailings release α particles to decay into radon atoms. Under the effect of nuclear recoil and radon emanation, some radon atoms leave the solid lattices and enter the interconnected pores between particles, becoming freely mobile radon atoms.

The second stage is migration of radon. Under the effect of diffusion and permeation, freely mobile radon atoms within uranium mill tailing sand particles continuously migrate upward through channels such as pores and microcracks, reaching the red soil layer.

The third stage is exhalation of radon. Freely mobile radon atoms within the red soil layer continue their upward migration, releasing to the external environment from the surface of the cover soil.

2.2. Calculation Model of the Radon Exhalation Rate. Figure 2 shows the schematic of radon exhalation from the uranium mill tailing covering soil under wetting−drying cycles. The local static method is used to measure the change of radon concentration on the beach surface of uranium mill tailing impoundments under wetting−drying cycles. This method can complete sampling, measurement, and other operations after radon collection in a relatively short time.

The formula[25] for calculating the surface radon exhalation rate of the uranium mill tailing covering soil is as follows

$$\frac{dC}{dt} = \frac{JS}{V} - \lambda C - RC \tag{1}$$

where C is the accumulated radon concentration within the radon collection hood within time t, Bq/m^3; t is the radon collection time, s; J is the radon exhalation rate of uranium mill tailing covering soil, Bq/(m^2·s); S is the base area of the radon collection hood, m^2; V is the volume of the radon collection hood, m^3; λ is the decay constant of radon, 2.1×10^{-6}, s^{-1}; R is the rate of radon leakage and back-diffusion, s^{-1}; $\frac{JS}{V}$ is the radon concentration change caused by radon exhalation into the radon collection hood per unit of time, Bq/(m^3·s); λC is the radon concentration change caused by decay of radon within the radon collection hood per unit of time, Bq/(m^3·s); and RC is the radon concentration change caused by leakage and back-diffusion of radon within the radon collection hood per unit of time, Bq/(m^3·s).

Substituting the initial condition $t = 0$ and $C = C_0$ into eq 1, we obtain

$$J = \frac{(\lambda + R)V}{S} \cdot \frac{(C - C_0 e^{-(\lambda+R)t})}{(1 - e^{-(\lambda+R)t})} \tag{2}$$

https://doi.org/10.1021/acsomega.4c00374
ACS Omega 2024, 9, 19295−19310

Under the condition of a very short radon collection time and a low initial radon concentration C_0, $(\lambda + R)t \ll 1$, $e^{-(\lambda+R)t} \approx 1 - (\lambda + R)t$, eq 2 can be approximated as

$$J = \frac{V}{St}(C - C_0) \tag{3}$$

Given the completion of radon collection in a relatively short time, radon concentration within the radon collection hood essentially exhibits a linear growth with time. Therefore, eq 3 can be simplified to

$$J = \frac{Vk}{S} \tag{4}$$

where k is the slope of the fitted curve, which represents the variation of the accumulated radon concentration over time, Bq/(m^3·s).

2.3. Crack Image Analysis System. The crack image analysis system (CIAS) is employed for the automatic identification and quantitative analysis of cracks and blocks in a crack image, allowing for the rapid extraction of geometric information such as number of cracks, individual crack length, width, and area. The process of obtaining surface crack indicators of the uranium mill tailing covering soil involves the following steps. First, the image is preprocessed by greyscale conversion, binarization, fixed-point impurity removal, and crack bridging. They aim to correct, reasonably restore, and enhance crack information in the crack image. Subsequently, the soil block is identified and quantified and the relevant parameters are recorded. Finally, the crack is identified and quantified. The crack is smoothed, skeletonized, and cropped, followed by crack recognition and recording the relevant parameters.

The formula for calculating the surface crack ratio of the uranium mill tailing covering soil is as follows

$$R = \frac{S_1}{S_2} \tag{5}$$

where R is the surface crack ratio,; S_1 is the total area of cracks in pixels, px; and S_2 is the total area in pixels, px.

2.4. Calculation Model of Cumulative Damage Degree. Application of ultrasonic detection technology to measure the ultrasonic wave velocity within the uranium mill tailing covering soil is significant for evaluating the soil integrity. Using longitudinal wave velocity as an independent variable, the cumulative damage degree[40] is employed to quantify the extent of damage within the uranium mill tailing covering soil during the wetting−drying cycling process.

$$D = 1 - \left(\frac{v_p}{v_0}\right)^2 \tag{6}$$

Here, D is the cumulative internal damage degree of the uranium mill tailing covering soil; v_p is the longitudinal wave velocity within the uranium tailing covering soil after a certain number of wetting−drying cycles, m/s; and v_0 is the initial longitudinal wave velocity within the uranium tailing covering soil.

2.5. Grey Relational Analysis. The grey system theory is primarily devoted to addressing issues where data is limited and information is incomplete. Grey relational analysis is a method of inferring the evolutionary pattern through known information with a system. It measures the closeness of the relationship between two factors by comparing the similarity of their developmental trends. The steps for calculating the grey relational degree are as follows.

x_0 is the reference sequence that determines the overall behavior of a reaction system, and x_1, x_2, x_3... are the comparative sequences that influence a system's behavior. Then, dimensionless processing is conducted on the reference sequence and the comparative sequence. The calculation formula for min−max standardization is as follows

$$x_{ij} = \frac{X_{ij} - \min X_{ij}}{\max X_{ij} - \min X_{ij}} (i = 1, 2, ..., n; j = 1, 2, ..., m) \tag{7}$$

where x_{ij} is the standardized value of data j in data set i, X_{ij} is the actual value of data j in data set i, minX_{ij} is the minimum value in data set i, and maxX_{ij} is the maximum value in data set i.

The calculation formula of the grey relational coefficient for the reference sequence and the comparative sequence[41] is as follows

$$\xi_i(j) = \frac{\min_i \min_j |x_0(j) - x_i(j)| + \rho \max_i \max_j |x_0(j) - x_j(j)|}{|x_0(j) - x_i(j)| + \rho \max_i \max_j |x_0(j) - x_i(j)|} \quad (i = 1, 2, ..., n; j = 1, 2, ..., m) \tag{8}$$

where $\xi_i(j)$ is the grey relational coefficient between the comparative sequence i and the reference sequence; $\min_i \min_j |x_0(j) - x_i(j)|$ is the two-level minimum difference; ρ is the grey resolution coefficient with a value in the range of [0,1], typically taking $\rho = 0.5$; $\max_i \max_j |x_0(j) - x_i(j)|$ is the two-level maximum difference; and $|x_0(j) - x_i(j)|$ is the two-level difference.

The calculation formula of the grey relational degree for the reference sequence and the comparative sequence is as follows

$$r_i = \frac{1}{N} \sum_{j=1}^{m} \xi_i(j) (i = 1, 2, ..., n; j = 1, 2, ..., m) \tag{9}$$

where r_i is the grey relational degree between the comparative sequence i and the reference sequence, N is the number of data for the grey relational coefficient between the comparative sequence i and the reference sequence, and $\sum_{j=1}^{m} \xi_i(j)$ is the sum of the grey relational coefficients between the comparative sequence i and the reference sequence.

3. MATERIALS AND METHODS

3.1. Sample Preparation. The samples of uranium mill tailing sand from an exposed section of a uranium mill tailing impoundment in the southern region of China were collected at a depth of 0−1.5 m. The radium specific activity of samples was 8.66×10^3 Bq/kg, and the porosity was 58%. First, samples were sieved through a 2 mm screen to remove impurities. Subsequently, samples were placed into a forced-air-drying oven with a drying temperature of 105 ± 5 °C and dried for 24 h. They were then stored in a sealed condition. The particle size composition of uranium mill tailing sand is shown in Table 1.

Chemical composition of the uranium mill tailing sand is shown in Table 2.

The red soil samples from a specific city in southern China were sieved through a 2 mm screen to remove impurities.

https://doi.org/10.1021/acsomega.4c00374
ACS Omega 2024, 9, 19295−19310

Table 1. Particle Size Composition of Uranium Mill Tailing Sand

standard screen level	mesh	aperture (mm)	sample quality (g)	percentage (%)
1	18	1	30	1.5
2	35	0.5	471	23.55
3	50	0.355	468.2	23.41
4	65	0.25	347.1	17.36
5	200	0.075	580.9	29.04
6	325	0.045	63.1	3.16
7	>325	<0.045	39.7	1.98

Subsequently, samples were placed in a forced-air-drying oven with a drying temperature of 105 ± 5 °C and dried for 24 h. They were then stored in a sealed condition. Basic physical properties of the red soil are shown in Table 3.

3.2. Preparation of the Covering Soil Model of Uranium Mill Tailings. We conducted a field investigation to study the hydrogeological condition of the uranium mill tailing impoundments located in southern China. We learned the progress of the decommissioning treatment project of the uranium mill tailing impoundments and obtained parameters such as the average thickness of each layer of the beach surface cover system of uranium mill tailing impoundments. The focus of the paper is on the unsaturated covering soil layer on the beach surface of uranium mill tailing impoundments. The saturated moisture content of the red soil used in this experiment was 60.1%. Therefore, the control point moisture content was set as 30%. The three amplitudes of wetting−drying cycles were 30 ± 10, 30 ± 15, and 30 ± 20%. This ensured that the maximum amplitude of wetting−drying cycles could cover the range of unsaturated moisture content of the red soil and be accurately monitored by soil temperature and the humidity sensor. Based on a similar condition, the accumulated thickness of the covering soil model of uranium mill tailings was calculated. The model was divided into two layers from the bottom to the top. The first layer was uranium mill tailing sand with a saturated water content, piled to a height of 500 mm. The second layer was compacted red soil with a water content of 30%, piled to a height of 100 mm. The specific steps for preparing the model are as follows.

(1) The uranium mill tailing sand is loaded. The uranium mill tailing sand is divided into 10 equal portions and filled into the test column. The uranium mill tailing sand is compacted to a height of 50 mm in a flat plane using a compaction tool during each filling.
(2) The uranium mill tailing sand layer is infiltrated and then immersed repeatedly, which is 500 mm high, in distilled water until water accumulated on the surface. Then, a straw is used to remove excess water.
(3) The uranium mill tailing sand layer is allowed to settle. The test box is left open at the top and placed in a well-ventilated area for a 15 day settling period.
(4) The airtightness of the radon exhalation measurement device is checked. The radon collection hood is connected tightly to the test column using screws. The outlet hole of the radon collection hood is connected to the upper end of the drying tube via the guide tube. The lower end of the drying tube is connected to the inlet of the RAD7 radon detector. The outlet of the radon detector is connected to the inlet hole of the radon collection hood. The reserved holes are sealed. Soapy water is applied to the joint between the radon collection hood and the guide tube, and air is passed into the radon collection space to check for the presence of bubbles. If there are no bubbles, it indicates good airtightness of the device. The radon concentration measurement device is shown in Figure 3.
(5) The radon concentration in the exposed uranium mill tailing sand is measured. The RAD7 radon detector is started and run in the purification mode for 30 min to achieve an internal relative humidity below 10% RH. The measurement time is set to 10 min, and the number of cycles is set to 10. Then, measurement is initiated.
(6) Red soil is prepared. The red soil is prepared with an initial water content of 30% using distilled water. It is stirred uniformly and sealed for 1 day.
(7) The red soil is loaded. The red soil is divided into five equal portions and filled into the test column. The red soil is compacted to a height of 20 mm in a flat plane using a compaction tool during each filling. The soil temperature and humidity sensor probe is inserted into the side of the test column and edge gaps are sealed with a tape. After calculation, the compaction degrees of the three models were 0.894, 0.91, and 0.906.
(8) The test box is sealed with a plastic wrap and placed in a location not exposed to direct sunlight for 3 days.
(9) The initial surface crack image of the compacted red soil is captured using a camera.
(10) The initial internal ultrasonic wave velocity of the compacted red soil is measured. The nonmetal ultrasonic detection analyzer is turned on, the rock defect detection mode is entered, and the measuring distance is set to 200 mm. Three samples are collected, and the average value is taken.
(11) The airtightness of the radon exhalation measurement device is checked.
(12) The radon concentration is measured after covering the soil, and the RAD7 radon detector is purified.
(13) The radon reduction efficiency is calculated after covering the soil. The radon exhalation rate based on the radon concentration before and after covering the uranium mill tailing sand with soil is calculated. Then, the radon reduction efficiency is calculated after covering the soil based on them. Radon reduction efficiencies of the three models were 98.3, 99.7, and 98.4%.

3.3. Experimental Implementation. The uranium mill tailing impoundments in southern China are located in a region with sufficient heat, abundant precipitation, and concurrent rainfall and heat. Intermittent rainfall is also a common occurrence in this area. In recent years, there have been frequent episodes of sustained high temperature in this

Table 2. Chemical Composition of the Uranium Mill Tailing Sand

constituent	SiO_2	Al_2O_3	MgO	Fe_2O_3	CrO_2	TiO	K_2O	CaO	U
quality content (%)	85.41	10.82	1.36	1.14	0.55	0.32	0.18	0.15	0.07

https://doi.org/10.1021/acsomega.4c00374
ACS Omega 2024, 9, 19295−19310

Table 3. Basic Physical Properties of Red Soil

particle composition (%)					
2−0.075 mm	0.075−0.005 mm	<0.005 mm	saturated moisture content (%)	relative density	maximum dry density (g/cm^3)
97.35	1.6	1.05	60.1	2.69	1.77

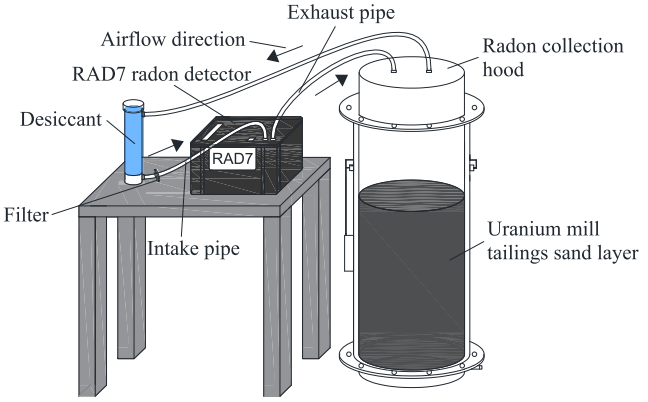

Figure 3. Radon concentration measurement device.

region, with the air temperature reaching up to 40 °C. The soil temperature in the region, from 0 to 50 cm depth, ranges between 21 and 23 °C.[42] In the experiment, a long arc xenon lamp that simulated sunlight was used to provide a temperature of 40 °C. The automatic heating temperature of the insulation heating belt was set to 22 °C to provide a stable temperature for the cover soil layer. A water spraying device that simulated rainfall was used to change the soil moisture content of the cover soil layer. The experimental device simulating the wetting−drying cycles is shown in Figure 4.

Wang et al.[37] quantitatively analyzed the crack area rate, the total crack length, and the average crack width of the soil through wetting−drying cycle tests. They found that the development of soil cracks was basically completed and the structure tended to be stable after six wetting−drying cycles. Therefore, the paper proposed seven wetting−drying cycles under each amplitude. The control point moisture content was set at 30% with three wetting−drying cycle amplitudes of 30 ± 10, 30 ± 15, and 30 ± 20%. One set of blank control experiments was proposed for each amplitude, and a total of seven wetting−drying cycles were conducted. The schematic of the design of the wetting−drying cycle experimental plan is shown in Figures 5 and 6.

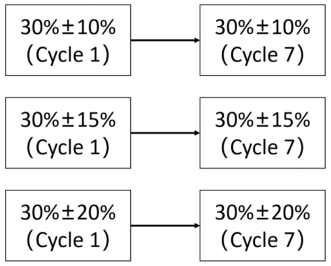

Figure 5. Diagram of wetting−drying cycles.

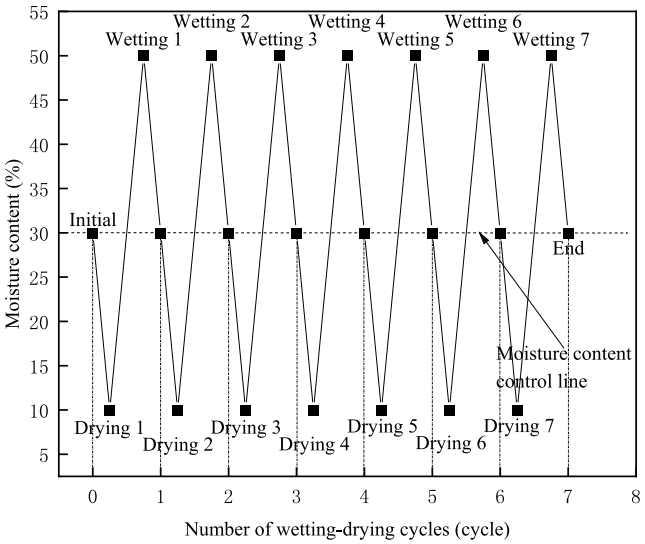

Figure 6. Schematic diagram of the wetting−drying cycle process (alternation amplitude: 30% ± 20%, alternation number: 7).

The experimental plan is shown in Table 4.

Taking the second group of experiments in the experimental plan as an example, the specific steps are as follows.

(1) Wetting−drying cycle experiments are conducted. First, a desiccation treatment on the compacted red soil is performed. The long arc xenon lamp is turned on to

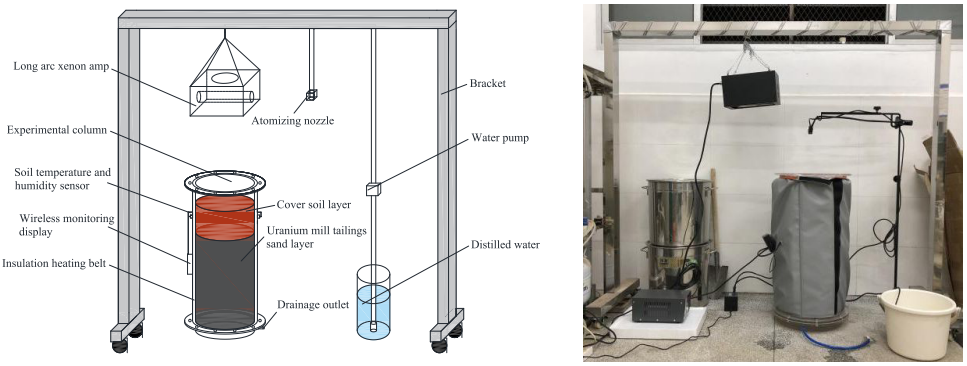

(a) Schematic (b) Physical

Figure 4. Experimental device simulating the wetting−drying cycles.

https://doi.org/10.1021/acsomega.4c00374
ACS Omega 2024, 9, 19295−19310

Table 4. Wetting−Drying Cycle Experimental Plan

experimental group number	control point moisture content	amplitude of wetting−drying cycles	moisture content variation range	number of wetting−drying cycles
1	30%			0
2	30%	±10%	20−40%	1
3	30%	±10%	20−40%	2
4	30%	±10%	20−40%	3
5	30%	±10%	20−40%	4
6	30%	±10%	20−40%	5
7	30%	±10%	20−40%	6
8	30%	±10%	20−40%	7
9	30%			0
10	30%	±15%	15−45%	1
11	30%	±15%	15−45%	2
12	30%	±15%	15−45%	3
13	30%	±15%	15−45%	4
14	30%	±15%	15−45%	5
15	30%	±15%	15−45%	6
16	30%	±15%	15−45%	7
17	30%			0
18	30%	±20%	10−50%	1
19	30%	±20%	10−50%	2
20	30%	±20%	10−50%	3
21	30%	±20%	10−50%	4
22	30%	±20%	10−50%	5
23	30%	±20%	10−50%	6
24	30%	±20%	10−50%	7

vertically illuminate the compacted red soil and activate the heating function of the insulation heating belt. When the soil temperature and the humidity sensor displayed a decrease in the moisture content to 10%, the lamp is turned off. Then, a humidification treatment is performed on the compacted red soil. The water spraying device is opened and water is sprayed onto the compacted red soil from directly above. When the sensor showed an increase in the moisture content to 50%, the sprinkler was closed. Finally, a desiccation treatment is performed on the compacted red soil again. The lamp is used to reduce the moisture content of the compacted red soil to 30%.

(2) The image of surface cracks in the compacted red soil is captured using a camera.
(3) The internal ultrasonic wave velocity of the compacted red soil is measured. The nonmetal ultrasonic detection analyzer is configured with a measurement distance of 200 mm, and three samples are collected, followed by calculating the average value.
(4) The airtightness of the radon measurement device is checked.
(5) The radon concentration is measured, and the RAD7 radon detector is purified.

The specific processes of one group of wetting−drying cycle experiments are shown in Figure 7.

4. RESULTS AND DISCUSSION

The surface crack images of the uranium mill tailing covering soil were imported into CIAS to obtain soil surface crack indicator data including the number of cracks, total length of cracks, average width of cracks, and surface crack ratio. The internal ultrasonic wave velocity of the covering soil was used in the corresponding formula to calculate the cumulative damage degree. The radon concentration on the surface of the covering soil was used in the corresponding formula to

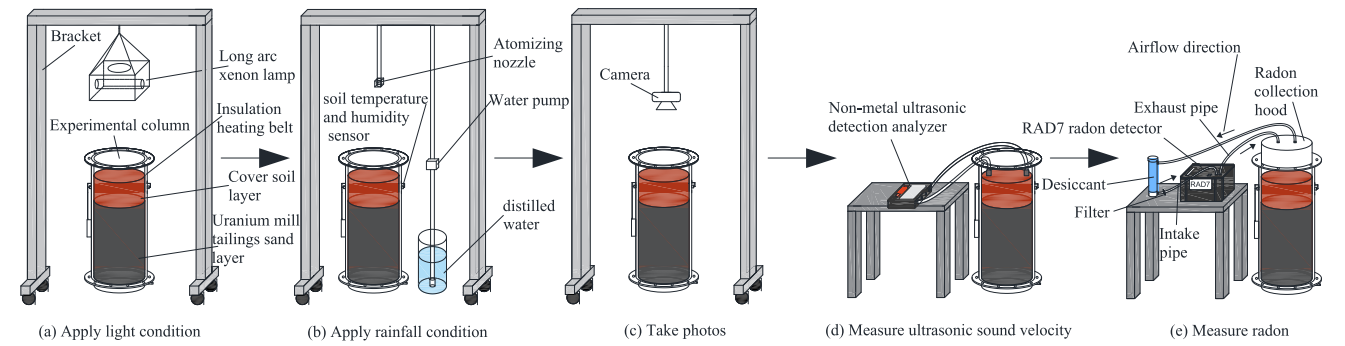

(a) Schematic

(b) Physical

Figure 7. Experimental process of wetting−drying cycles.

https://doi.org/10.1021/acsomega.4c00374
ACS Omega 2024, 9, 19295−19310

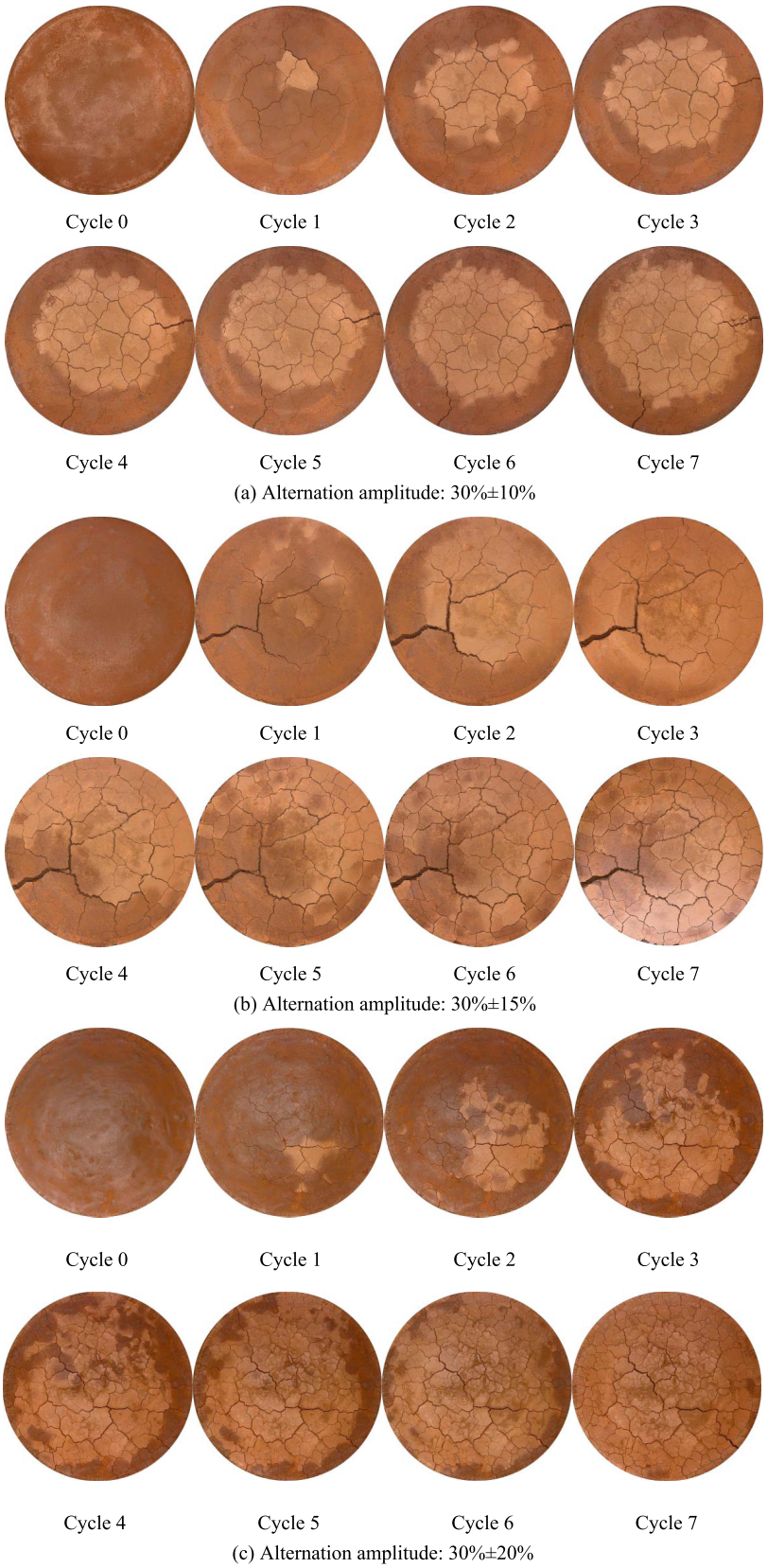

Figure 8. Surface crack images in the cover soil under different numbers of wetting−drying cycles.

calculate the radon exhalation rate. Original images of surface cracks in uranium mill tailing covering soil are shown in Figure 8.

4.1. Analysis of Surface Crack Indicators in the Cover Soil. *4.1.1. Analysis of Number of Cracks in the Cover Soil.* The curve change of the number of surface cracks in the uranium mill tailing covering soil under three amplitudes of

https://doi.org/10.1021/acsomega.4c00374
ACS Omega 2024, 9, 19295−19310

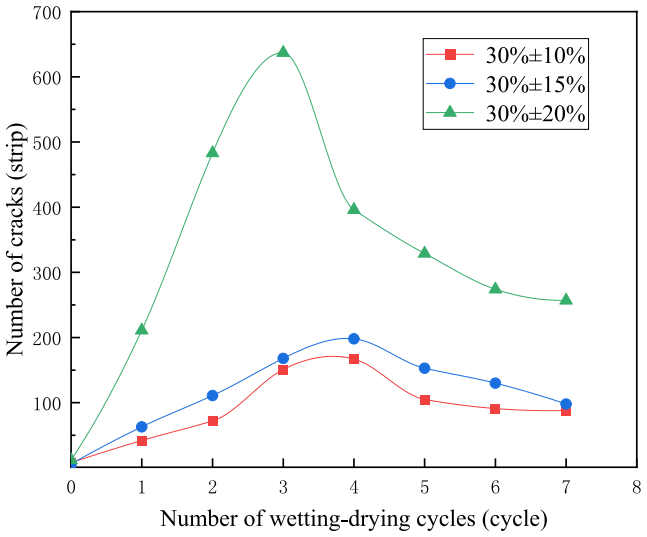

Figure 9. Variation of crack number with the number of wetting−drying cycles.

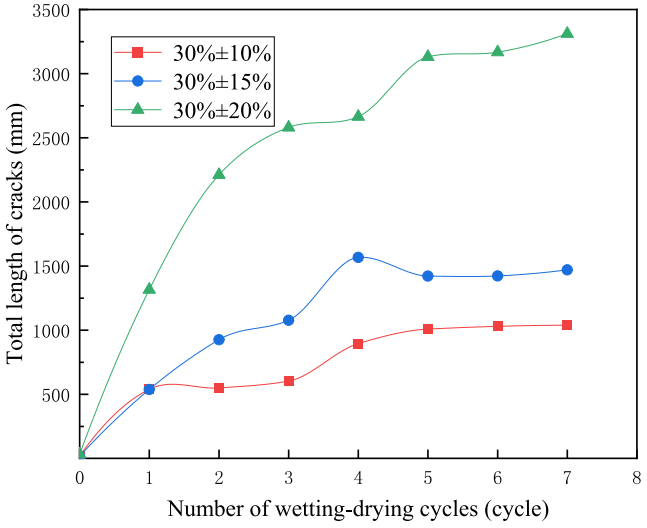

Figure 10. Variation of total crack length with the number of wetting−drying cycles.

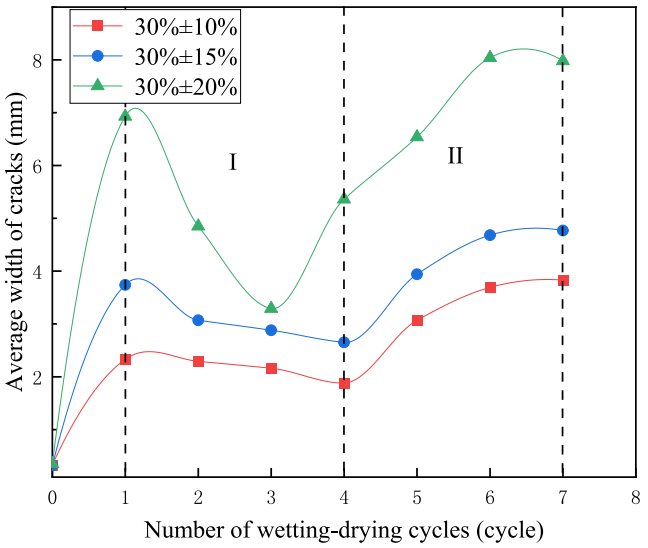

Figure 11. Variation in average crack width with the number of wetting−drying cycles.

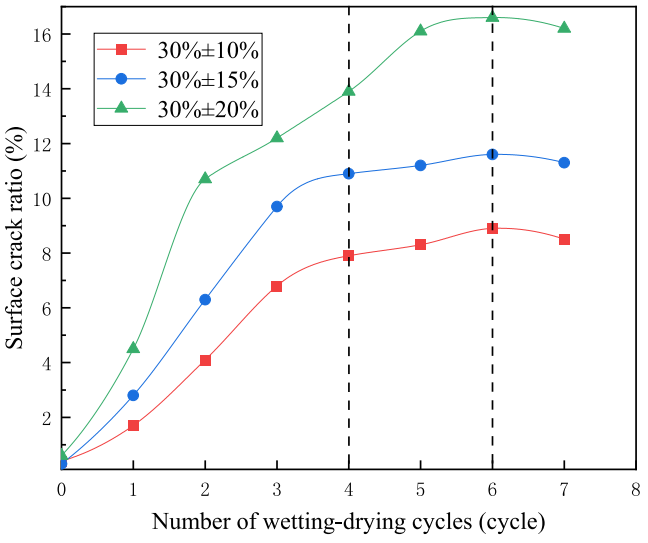

Figure 12. Variation of the surface crack ratio with the number of wetting−drying cycles.

wetting−drying cycles is similar. They show a two-stage change, transitioning from a linear ascent to a linear descent, as shown in Figure 9.

We take the curve of the wetting−drying cycle amplitude of 30 ± 15% as an example for analysis. During the early-to-mid-stage of wetting−drying cycles (numbers 0−4), the degree of cracking on the surface of the uranium mill tailing covering soil was relatively severe. A large number of microcracks appeared after the first wetting−drying cycle. As the alternation continued, initial cracks further developed and secondary cracks gradually emerged. They were all leading to a continuous increase in the number of cracks. In the mid-to-late stage of wetting−drying cycles (numbers 4−7), the degree of surface cracking gradually transitioned to a stable stage. The generation rate of microcracks slowed down or even stopped. Some microcracks merged with other cracks to form the main cracks. At this point, the number of cracks showed a decreasing trend.

During the dehumidification process of the uranium mill tailing covering soil, the surface of the soil was directly heated, causing its dehydration rate to be noticeably faster than that at the bottom. The surface of the soil lost moisture generously and rapidly, leading to contraction, while the bottom of the soil lost moisture less slowly, restraining surface contraction. As a result, a certain tensile stress formed on the surface of the soil. When this stress exceeded the strength of the soil, cracks were formed. With a constant soil strength, the greater the wetting−drying cycles' amplitude (for example, 30 ± 20%), the larger the tensile stress formed on the soil surface, resulting in a more dense and complex network of microcracks. Therefore, the larger the alternation amplitude, the faster the number of crack increase and the higher the peak value.

4.1.2. Analysis of the Total Length of Cracks in Cover Soil. The total length of surface cracks in the uranium mill tailing covering soil under three amplitudes of wetting−drying cycles shows a "stair-step" increase with the increase in number of wetting−drying cycles. This pattern involves a significant increase, followed by a slight increase, and then tends to be stable, as shown in Figure 10.

https://doi.org/10.1021/acsomega.4c00374
ACS Omega 2024, 9, 19295−19310

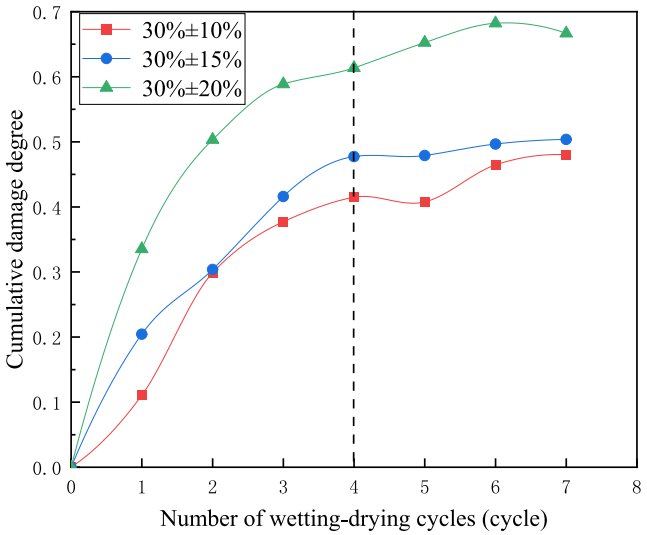

Figure 13. Variation of the cumulative damage degree with the number of wetting−drying cycles.

Table 5. Original Experimental Data

experimental group number	number of cracks (strip)	total length of cracks (mm)	average width of cracks (mm)	surface crack ratio (%)	radon exhalation rate (Bq/(m²·s))
4	151	602.59	2.16	6.8	0.0274
5	167	894.92	1.88	7.9	0.0253
6	105	1008.41	3.07	8.3	0.0275
7	91	1029.57	3.69	8.9	0.0316
8	88	1038.14	3.83	8.5	0.0298
12	168	1077.72	2.88	9.7	0.0664
13	198	1567.35	2.65	10.9	0.0713
14	153	1422.13	3.94	11.2	0.0892
15	130	1422.53	4.68	11.6	0.0951
16	98	1470.15	4.77	11.3	0.0899
20	637	2579.99	3.29	12.2	0.5332
21	396	2664.37	5.36	13.9	0.6278
22	329	3131.07	6.54	16.1	0.7623
23	274	3167.44	8.04	16.6	0.7819
24	257	3311.29	7.98	16.2	0.6893

Table 6. Grey Relational Degree between the Radon Exhalation Rate and Various Indicators

index	number of cracks	total length of cracks	average width of cracks	surface crack ratio
grey relational degree	0.7487	0.7597	0.7561	0.7652

In the early stage of wetting−drying cycles, the total length of cracks was mainly influenced by microcracks. During this period, the soil surface had sufficient space for water loss and each dehumidification cycle generated a large number of short and narrow microcracks, leading to a significant increase of the total length of cracks. In the middle stage of wetting−drying cycles, the total length of cracks was mainly influenced by major cracks. Due to space limitation caused by water loss at the soil surface, the growth rate of microcracks slowed down after each dehumidification cycle, resulting in a minor increase in the total length of cracks. In the late stage of wetting−drying cycles, almost all cracks had developed and few new cracks were formed, leading to a stabilization of the total length of cracks.

In the process of dehumidification, the greater the amplitude of wetting−drying cycles, the greater the evaporation of soil surface moisture. The tensile stress generated on the soil surface became larger and its action time became longer, which promoted the initiation and expansion of cracks. Therefore, with a constant number of wetting−drying cycles, the total length of cracks increased as the amplitude of wetting−drying cycles increased.

4.1.3. Analysis of the Average Width of Cracks in Cover Soil. After the first wetting−drying cycles, the average width of surface cracks in uranium mill tailing covering soil under three amplitudes of wetting−drying cycles generally shows a two-stage change, transitioning from a linear decrease to a linear increase, as shown in Figure 11.

After the first wetting−drying cycles, cracks occurred on the initial surface of the covering soil model of uranium mill tailings, resulting in an average width of cracks. During the early-to-mid-stage of wetting−drying cycles (numbers 1−4), the average width of cracks was primarily influenced by microcracks. As the number of wetting−drying cycles increased, the number of microcracks on the soil surface increased, but most newly formed microcracks did not fully develop and had a small width, resulting in a decrease in the average width of cracks. In the mid-to-late stage of wetting−drying cycles (numbers 4−7), the average width of cracks was mainly influenced by major cracks. Due to limitation of the water loss space, only a few microcracks continued to develop into major cracks. Most microcracks merged with others to form major cracks. These factors contributed to an increase of the average width of cracks.

In the process of dehumidification, when the number of alternating wetting−drying cycles was constant, the larger the amplitude of wetting−drying cycles, the longer the development time of cracks, leading to a wider average crack width.

4.1.4. Analysis of the Surface Crack Ratio in Cover Soil. The variation in the surface crack rate in the uranium mill tailing covering soil under three amplitudes of wetting−drying cycles can be generally divided into three stages: stage I is the development of microcracks, characterized by a rapid increase of the surface crack rate; stage II is the development of major cracks, characterized by a stable increase of the surface crack rate starting from the fourth wetting−drying cycle; and stage III is the stable recession of cracks, characterized by a slight decrease of the surface crack rate starting from the sixth wetting−drying cycle, as shown in Figure 12.

We take the curve with a wetting−drying cycle amplitude of 30 ± 15% as an example for analysis. In stage I, which occurred in the early-to-mid-stage of wetting−drying cycles (numbers 0−4), a densely distributed and complex network of microcracks appeared on the surface of the uranium mill tailing covering soil. During the dehumidification process, there was a spatial distribution difference in the evaporation rate of soil moisture. The dehumidification rate at the soil surface was significantly greater than that at the bottom. The soil surface was directly heated, causing a rapid evaporation of a large amount of free water. The soil surface began to shrink. However, the soil bottom lost almost no water. Thus, a certain tensile stress was formed on the soil surface, inhibiting surface shrinkage. When the tensile stress on the soil surface exceeded the strength of the soil, microcracks occurred on the surface. During the humidification process, the soil surface swelled as it

https://doi.org/10.1021/acsomega.4c00374
ACS Omega 2024, 9, 19295−19310

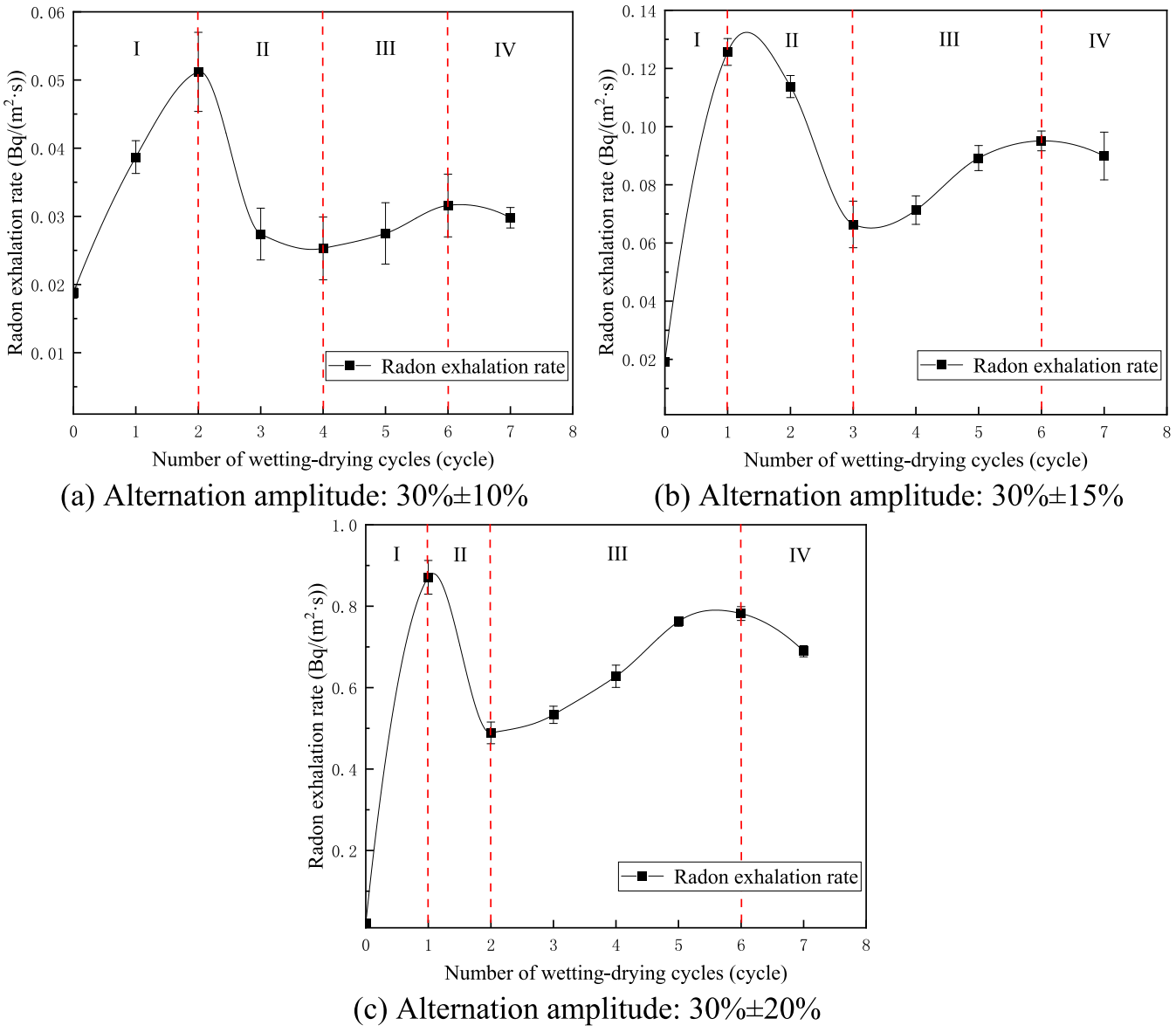

Figure 14. Variation of the radon exhalation rate with the number of wetting−drying cycles.

absorbed water, partially closing some microcracks; however, the strength of the soil did not fully recover to its original level. When humidifying again, the cracks would reopen along the weak position and spread to the surrounding. At this time, there was sufficient space for water loss on the soil surface, resulting in a rapid increase of the surface crack rate.

In stage II, which occurred in the mid-to-late stage of wetting−drying cycles (numbers 4−6), surface microcracks of the uranium mill tailing covering soil decreased and major cracks increased. As the wetting−drying cycles progressed, the soil surface was divided into many small pieces. A large amount of capillary water was transported from the soil bottom to the surface through channels provided by initial cracks, reducing the gradient of moisture content between the surface and the bottom of the soil. The potential energy reserve of tensile stress on the soil surface also decreased. The effect of wetting−drying cycles was no longer significant. Due to the limited space for water loss on the soil surface, only a few microcracks developed into major cracks, while most microcracks merged with other cracks to form major cracks. Hence, the surface crack rate showed a slow increase.

In stage III, which occurred in the final stage of wetting−drying cycles (numbers 6−7), almost all cracks had developed and even a few microcracks had closed. At this point, the structure of the soil stabilized after multiple wetting−drying cycles. The space of soil dehumidification reversed. Free water on the soil surface rapidly dissipated, and the development of cracks basically came to a stop. The soil bottom continued to lose water. Pressure stress was formed on the soil surface, promoting surface shrinkage. Some microcracks were closed by compression, and the width of major cracks also decreased to some extent, resulting in a slight decrease of the surface crack rate.

With a constant number of wetting−drying cycles, the larger the amplitude of wetting−drying cycles, the greater the influence of wetting−drying cycles on the development of soil surface cracks, leading to a higher surface crack rate.

4.2. Analysis of Cumulative Internal Damage in Cover Soil. The internal cumulative damage of the uranium mill

https://doi.org/10.1021/acsomega.4c00374
ACS Omega 2024, 9, 19295−19310

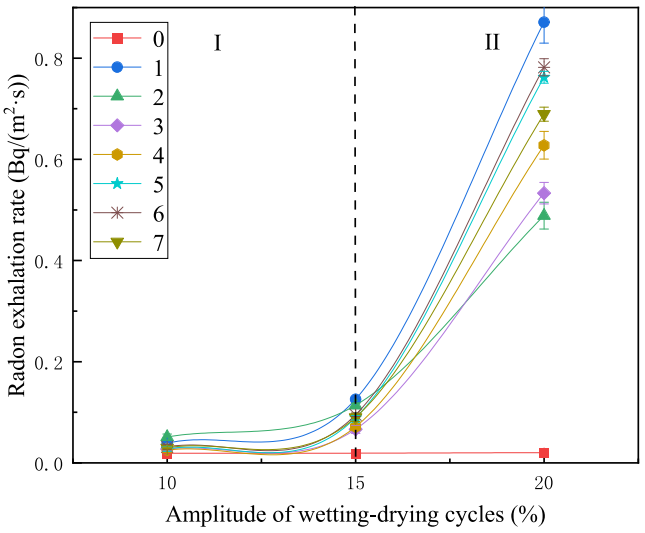

Figure 15. Variation of the radon exhalation rate with the amplitude of wetting−drying cycles.

tailing covering soil under three amplitudes of wetting−drying cycles generally shows a two-stage change, characterized by rapid growth followed by a stable phase, as illustrated in Figure 13.

Jiang et al.[40] pointed out that when the internal cumulative damage degree of a material reached 0.19, it signified the formation of damage. After the second wetting−drying cycle, the internal cumulative damage degree of the uranium mill tailing covering soil had exceeded 0.19, indicating a significant degree of structural damage due to wetting−drying cycles. The increase in the number of wetting−drying cycles led to a notable change in the internal structure of the soil, manifested by a rapid increase in the cumulative damage degree. After the fourth wetting−drying cycle, the internal structure of the soil tended to stabilize, resulting in a slowed increase of the cumulative damage degree.

When the number of wetting−drying cycles was constant, the larger the amplitude of wetting−drying cycles, the more obvious the damage degree of wetting−drying cycles to the soil's internal structure, leading to a greater cumulative damage degree.

4.3. Grey Relational Analysis between the Radon Exhalation Rate and Surface Crack Indicators in Cover Soil. In the case of limited experimental data, to further clarify the influential degree of various surface crack indicators on the radon exhalation rate of the uranium mill tailing covering soil under wetting−drying cycles, grey relational analysis is used to quantitatively characterize the strength of correlation between the radon exhalation rate and the number of cracks, the total length of cracks, the average width of cracks, and the surface crack rate. During the first and second wetting−drying cycles, anomalous radon exhalation was mainly influenced by the initial cumulative radon exhalation in the uranium mill tailing covering soil layer. To minimize interference, experimental data from numbers 3−7 under each wetting−drying cycle amplitude with a total of 15 groups was selected for analysis, as shown in Table 5.

The radon exhalation rate is denoted as the reference sequence, represented by x_0. Number of cracks, total length of cracks, average width of cracks, and surface crack ratio are denoted as respective comparative sequences, represented by x_1, x_2, x_3, and x_4, respectively. The calculation result of grey relational degrees between the radon exhalation rate and each indicator is shown in Table 6.

Grey relational degrees between the radon exhalation rate and each surface crack indicator of the soil were all greater than 0.5, with a relatively small numerical difference. This indicated that the selected surface crack indicators of the soil had a certain scientific and rational basis, and they had a significant effect on the radon exhalation rate. The rank of grey relational degrees was as follows: surface crack rate > total length of cracks > average width of cracks > number of cracks. Compared to other surface crack indicators, surface crack rate had the greatest impact on the radon exhalation rate with a grey relational degree of 0.7652, while the number of cracks had the smallest impact on the radon exhalation rate with a grey relational degree of 0.7487. The variation in surface crack rate can be used to characterize the disturbance of surface cracks on radon retardation under wetting−drying cycles.

4.4. Effect of Wetting−Drying Cycles on the Radon Exhalation Rate in Cover Soil. *4.4.1. Effect of Number of Wetting−Drying Cycles on the Radon Exhalation Rate in Cover Soil.* Figure 14 displays the curves depicting the variation in the radon exhalation rate with the number of wetting−drying cycles under three amplitudes, showing a generally similar trend. The radon exhalation rate of the uranium mill tailing covering soil exhibits four distinct stages of variation: stage I shows a rapid increase, stage II shows a rapid decrease, stage III shows a gradual increase, and stage IV shows a stable or even slightly decreasing trend.

Stage I occurred in the early period of wetting−drying cycles. After filling each covering soil model of uranium mill tailings, it was sealed and allowed to stand for 3 days. During this period, freely mobile radon was continuously produced in the uranium mill tailing sand layer. Initial microcracks in the cover soil layer were few. Radon mainly diffused from the uranium mill tailing sand layer to the cover soil layer through pores. Radon was soluble in water, so most radon entering the cover soil layer dissolved in pore water. However, the diffusion rate of radon in water was less than 0.01% of that in air, inhibiting the diffusion of radon from the cover soil layer to the external environment. This resulted in a high initial cumulative radon concentration in the cover soil layer and a low surface radon exhalation rate. During the first dehumidification process, continuous light increased the environmental temperature and the pore water rapidly evaporated, releasing a large amount of freely mobile radon. Radon solubility decreased as the water temperature increased, releasing freely mobile radon. At this point, radon concentration in the cover soil layer rapidly increased, creating a significant radon concentration gradient with the external environment, leading to a rapid increase of the radon exhalation rate.

Stage II occurred in the middle period of wetting−drying cycles. The excessively high radon concentration in the cover soil layer gradually decreased to a normal level. Reduction in the radon concentration gradient between the inside and outside of the soil led to a decrease of the radon exhalation rate.

Stage III occurred in the late period of wetting−drying cycles. A large number of cracks formed on the surface of the cover soil layer, providing more channels for radon to diffuse to the external environment. At this point, the main migration channels for radon shifted from pores to cracks. The diffusion rate of radon in air was much faster than in soil. This implied

https://doi.org/10.1021/acsomega.4c00374
ACS Omega 2024, 9, 19295−19310

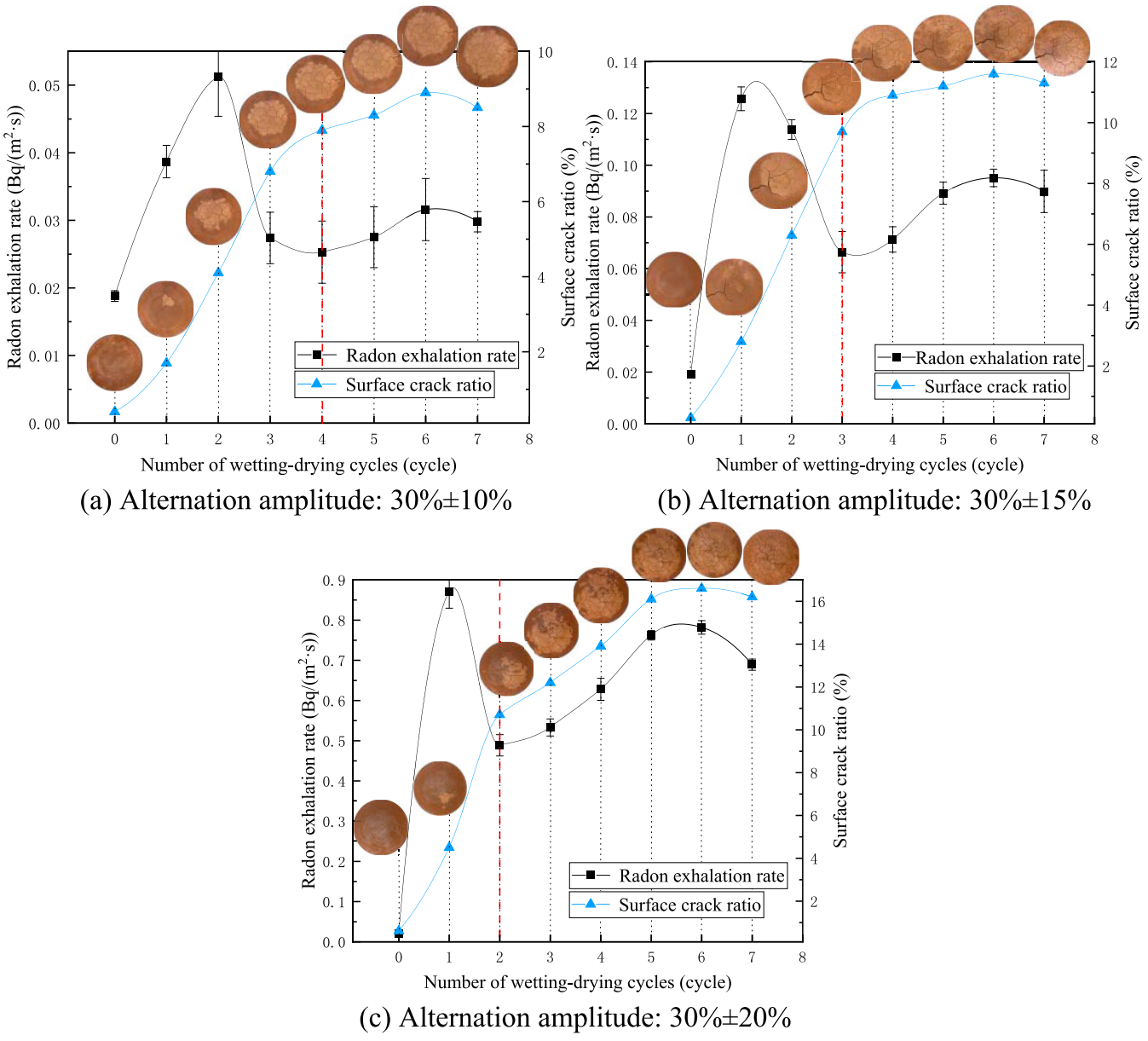

Figure 16. Variation of the radon exhalation rate and surface crack ratio with the number of wetting−drying cycles.

that the migration speed of radon in cracks was faster than in pores. Most cracks had developed and only a few continued to develop, resulting in a slow increase of the total number of cracks. This was reflected in a gradual increase of the radon exhalation rate.

Stage IV occurred in the final period of wetting−drying cycles. Almost all cracks had developed, and there were even partial closures of some microcracks. This led to a relative reduction in migration channels for radon compared to the previous stage. After many cycles of dehydration treatment, the surface structure of the cover soil was damaged and the effect of cohesive force resulted in the formation of compaction, reducing the migration channels for radon. Therefore, these caused a slight decrease of the radon exhalation rate.

4.4.2. Effect of Amplitude of Wetting−Drying Cycles on the Radon Exhalation Rate in Cover Soil. The radon exhalation rate shows an overall trend of gradually increasing to rapidly increasing under seven wetting−drying cycles, as illustrated in Figure 15.

The influence of wetting−drying cycles' amplitude on the radon exhalation rate was mainly reflected in the case when the alternating amplitude was larger, for example, 30 ± 20%. During the dehumidification process, a greater wetting−drying cycle amplitude led to increased evaporation of surface moisture in the uranium mill tailing covering soil. This generated a higher tensile stress on the soil surface, prompting formation of more cracks. Consequently, this provided additional migration channels for radon, resulting in a more rapid increase of the radon exhalation rate. Under the same environmental temperature, a larger wetting−drying cycles amplitude prolonged the dehumidification time, extending the duration of tensile stress on the soil surface. This prolonged stress duration contributed to an extended process of crack initiation and development, forming more well-established radon migration channels, thereby enhancing radon exhalation.

4.4.3. Effect of Surface Crack Ratio on the Radon Exhalation Rate in Cover Soil. Figure 16 indicates that, after the early-to-mid-stage of wetting−drying cycles, the curves of

https://doi.org/10.1021/acsomega.4c00374
ACS Omega 2024, 9, 19295−19310

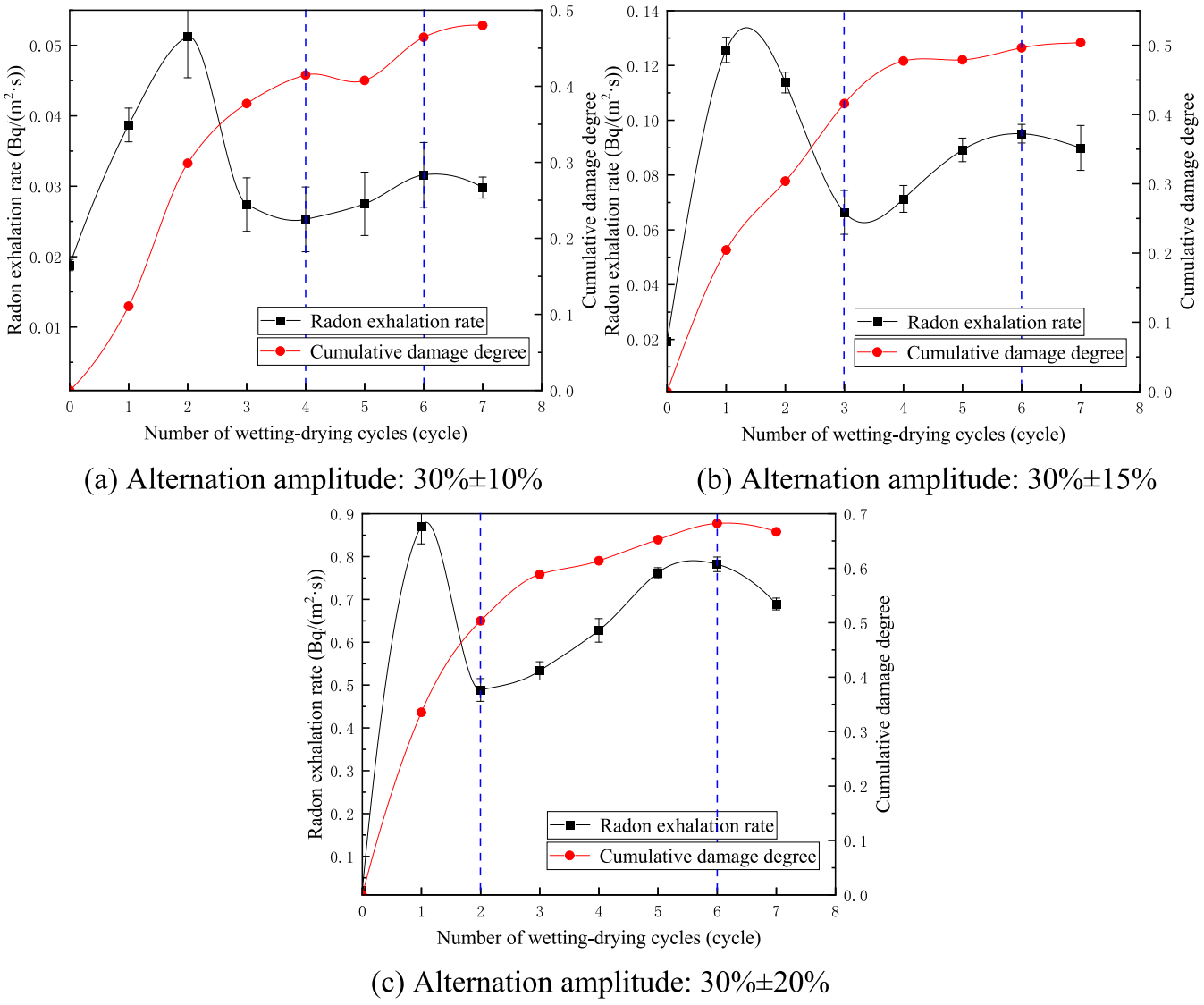

Figure 17. Variation of the radon exhalation rate and cumulative damage degree with the number of wetting−drying cycles.

the radon exhalation rate and surface crack ratio show a consistent trend with a gradual increase. By the seventh wetting−drying cycle, both exhibit a certain degree of convergence.

During the early-to-mid-stage of wetting−drying cycles, the anomalous radon exhalation was primarily influenced by the initial cumulative radon concentration in the uranium mill tailing covering soil layer. After this stage, as the irregularity and complexity of crack development increased, the surface crack ratio also became larger. The development of cracks provided more migration channels for radon. The main migration channels of radon shifted from pores to cracks, and the migration speed of radon in cracks was faster than in pores. Therefore, these were reflected in an increase of the radon exhalation rate. In the final stage of wetting−drying cycles, a few closed cracks led to a reduction in migration channels for radon, resulting in a decrease of the radon exhalation rate.

4.4.4. Effect of Cumulative Internal Damage on the Radon Exhalation Rate in Cover Soil. Figure 17 shows that from the early mid-stage to the late stage of wetting−drying cycles, both the radon exhalation rate and the cumulative damage degree exhibit a gradual increase.

We take the curve of wetting−drying cycle amplitude of 30 ± 15% as an example for analysis. During 0−3 wetting−drying cycles, the anomalous radon exhalation was primarily influenced by the initial accumulated radon concentration in the uranium mill tailing covering soil layer. In the initial cover soil layer, the soil structure was relatively intact and freely mobile radon primarily migrated through pores from the uranium mill tailing layer to the cover soil layer. During 3−6 wetting−drying cycles, the internal structure of the cover soil layer was noticeably damaged and some cracks extended deeper and farther, providing advantageous migration channels for radon. At this point, the primary migration channel for radon gradually shifted to the cracks, reducing the time for radon migration to the cover soil layer, thereby promoting radon emanation. After the seventh wetting−drying cycle, the radon exhalation rate slightly decreased and the cumulative damage degree showed a small increase, indicating that the change of the radon exhalation rate was also affected by other factors.

https://doi.org/10.1021/acsomega.4c00374
ACS Omega 2024, 9, 19295−19310

5. CONCLUSIONS

The paper analyzed the influence process of the number and amplitude of wetting−drying cycles on surface crack indicators, the cumulative damage degree, and the radon exhalation rate in the uranium mill tailing covering soil. Furthermore, it further explored the influence law of wetting−drying cycles on radon retardation in the uranium mill tailing covering soil through surface crack indicators and cumulative damage degree. The results can provide a useful reference for radon control and environmental assessment of the beach surface of uranium mill tailing impoundments. In summary, the following conclusions can be drawn.

(1) Various surface crack indicators collectively depicted the development process of surface cracks in the uranium mill tailing covering soil under wetting−drying cycles. With a constant amplitude of wetting−drying cycles, in the early-to-mid-stage of wetting−drying cycles, cracks were in the initiation phase, mainly generating microcracks characterized by a narrow width and greater abundance. In the mid-to-late stage of wetting−drying cycles, cracks entered the development completion phase, mainly generating main cracks characterized by a wide width and smaller abundance. After seven wetting−drying cycles, the total length of cracks exhibited a "stair-step" growth trend and the surface crack rate changed from rapid growth to stable growth and then to a slight decline.

(2) Cumulative damage degree in the uranium mill tailing covering soil showed a trend of rapid growth to stable growth with an increase in the number of wetting−drying cycles.

(3) According to grey relational analysis, compared to other surface crack indicators, the radon exhalation rate was the most closely correlated with the surface crack ratio.

(4) With a constant amplitude of wetting−drying cycles, the radon exhalation rate underwent four stages as the number of wetting−drying cycles increased: stage I was a rapid increase, stage II was a rapid decrease, stage III was a gradual increase, and stage IV was a stable or even slight decrease. When the number of wetting−drying cycles was constant, the radon exhalation rate correspondingly increased with the amplitude of wetting−drying cycles, particularly noticeable when the alternation amplitude was 30 ± 20%. From the early mid-stage to the late stage of wetting−drying cycles, the curves of the radon exhalation rate, surface crack ratio, and cumulative damage degree tended to be consistent, showing a gradual increase.

AUTHOR INFORMATION

Corresponding Author

Changshou Hong − *School of Resources, Environment and Safety Engineering, University of South China, Hengyang 421001, China*; Email: hongchangshou@163.com

Authors

Zhanyuan Zhang − *School of Resources, Environment and Safety Engineering, University of South China, Hengyang 421001, China*; orcid.org/0009-0009-0408-580X

Xiangyang Li − *School of Resources, Environment and Safety Engineering, University of South China, Hengyang 421001, China*

Hong Wang − *School of Resources, Environment and Safety Engineering, University of South China, Hengyang 421001, China*

Complete contact information is available at: https://pubs.acs.org/10.1021/acsomega.4c00374

Notes

The authors declare no competing financial interest.

ACKNOWLEDGMENTS

The authors gratefully acknowledge the financial support of the Natural Science Foundation of Hunan Province (2023JJ30495) and the Scientific Research Project of Education Department of Hunan Province (Grant No. 22B0463).

REFERENCES

(1) Wang, Z. Z. The environmental improvement of decommissioning uranium tailings impoundment. *Uranium Min. Metall.* **2003**, *22* (02), 95−99.

(2) Ye, Y. J.; Ding, D. X.; Luo, R.; Zhou, X. H.; Li, F. On the effect of volumetric water content on the radon exhalation rate of uranium tailings. *J. Saf. Environ.* **2012**, *12* (03), 124−126.

(3) Zhang, S.; Xiong, D. H.; Xiao, L.; Yang, D.; Zhang, B. J.; Wu, H. Influence of dry-wet cycling on soil properties. *Chin. J. Soil Sci.* **2017**, *48* (03), 762−768.

(4) Song, P. S.; Wang, J.; Chen, L.; Cao, B. Z.; Song, C. Y. Effect of wet-dry cycle on shear strength of compacted soil. *Res. Soil. Water Conserv.* **2021**, *28* (02), 74−79.

(5) Zhang, X. L.; Xu, L. C.; Wei, G. Z.; Cao, J.; Wang, E. Q. Minimization of radioactive solid wastes from uranium mining and metallurgy. *Uranium Min. Metall.* **2010**, *29* (04), 204−209.

(6) Leoni, G. L. M.; Almeida, M. D. S. S.; Fernandes, H. M. Computational modelling of final covers for uranium mill tailings impoundments. *J. Hazard. Mater.* **2004**, *110* (01), 139−149.

(7) Ferry, C.; Richon, P.; Beneito, A.; Robe, M. C. Evaluation of the effect of a cover layer on radon exhalation from uranium mill tailings: transient radon flux analysis. *J. Environ. Radioact.* **2002**, *63* (01), 49−64.

(8) Ghany, H. A. A.; El Aassy, I. E.; Ibrahim, E. M.; Gamil, S. H. White sand potentially suppresses radon emission from uranium tailings. *Radiat. Phys. Chem.* **2018**, *144*, 100−105.

(9) Tan, K. X.; Hu, H. Q.; Liu, Z. H.; Lv, J. W.; Xia, L. S. An exploration on the effectiveness of suppression of radon exhalation from uranium tailings by using different cover materials. *Acta Mineral. Sin.* **2012**, *32* (02), 233−237.

(10) Hong, C. S.; Xin, J. Y.; Li, S.; Wang, H.; Zhong, Y. M.; Li, X. Y.; Liu, Y. Effect of low content calcium lignosulfonate stabilized red clay on radon retardation. *Nonferrous Met. (Extr. Metall.)* **2022**, *2022* (10), 109−114.

(11) Li, X. D. Optimization analysis for cover thickness of uranium tailings impoundment. *Uranium Min. Metall.* **2001**, *20* (01), 28−34.

(12) Xie, T. F.; Li, J. L.; Wang, L. Parameter optimization of clay for radon attenuation covered on uranium tailings. *Radiat. Prot.* **2013**, *33* (04), 243−248.

(13) Dong, C. L. Study on radon eduction rate for remediation and decommissioning of uranium tailings impoundment. *Uranium Min. Metall.* **2001**, *20* (02), 93−102.

(14) Zhou, X. H.; Deng, W. H. Research on the effect of covered soil density on reducing radon emanation rate. *Uranium Min. Metall.* **2004**, *23* (01), 41−43.

(15) Xie, T. F.; Huang, D. F.; Zhang, S. L. Effect of compactness of covered soil on radon exhalation rate of uranium tailings. *Uranium Min. Metall.* **2010**, *29* (01), 33−36.

(16) Dai, X. W.; Chen, Y. F.; Chen, Y.; Wang, H.; Li, X. Y.; Hong, C. H.; Liu, Y. Effect of thickness and compaction degree of overburden soil on radon reduction for uranium tailings reservoir. *Sci. Technol.*

https://doi.org/10.1021/acsomega.4c00374
ACS Omega 2024, 9, 19295−19310

Nucl. Install. **2021**, *2021*, No. 9984939, DOI: 10.1155/2021/9984939.
(17) Li, X. J.; Cai, Z. M.; He, W. X.; Pan, J. L. Predication of moisture content distribution and radon emanation rate on uranium mill tailings surface. *Uranium Min. Metall.* **2005**, *24* (03), 145−148.
(18) Chen, Y. F.; Lin, D. Y.; Dai, X. W.; Wu, X. W.; Hong, C. H.; Liu, Y. Preliminary research on the evolution laws of overburden soil structure and its radon reduction ability for uranium tailings impoundment in extreme heat and insolation conditions. *J. Radioanal. Nucl. Chem.* **2021**, *330* (3), 1007−1015.
(19) Dai, J. Y.; Wang, M.; Zhou, S. L. Hybrid intelligent optimal selection research of cover materials in uranium tailing pile. *At. Energy Sci. Technol.* **2016**, *50* (07), 1329−1335, DOI: 10.7538/yzk.2016.50.07.1329.
(20) Ban, G. G.; Dai, J. Y. Simulation study of clay layer coverage governance of uranium tailings pile. *Ind. Saf. Environ. Prot.* **2019**, *45* (01), 83−86.
(21) Tan, K. X.; Liu, Z. H.; Xia, L. S.; Lv, J. W.; Hu, H. Q. The influence of fractal size distribution of covers on radon exhalation from uranium mill tailings. *Radiat. Meas.* **2012**, *47* (02), 163−167.
(22) Li, X. Y.; Liu, X. L.; Lan, M.; Liu, Y.; Hong, C. H.; Wang, H. Study on the influence of water content and particle size fractal distribution on radon exhalation in overburden soil layer of uranium tailings pond. *J. Saf. Environ.* **2021**, *21* (05), 2209−2215.
(23) Liu, X. L.; Li, X. Y.; Lan, M.; Liu, Y.; Hong, C. H.; Wang, H. Experimental study on permeability characteristics and radon exhalation law of overburden soil in uranium tailings pond. *Environ. Sci. Pollut Res.* **2021**, *28* (12), 15248−15258.
(24) Cai, Z. Q.; Zhang, Q. M.; Li, X. Y.; Lei, B.; Hong, C. H.; Shao, Z. Research on radon exhalation characteristics of uranium tailings with cover materials under the coupling load of low-frequency vibration and seepage gradient. *J. Radioanal. Nucl. Chem.* **2021**, *327* (02), 359−371.
(25) Hong, C. S.; Zhang, Z. Y.; Dai, X. W.; Chen, Y. F.; Chen, Y.; Lin, D. Y.; Chen, Z. X.; Liu, Y.; Li, X. Z.; Wang, H. Response law of radon exhalation rate from beach surface of uranium tailings pond under the earthquake-rainfall effect. *Min. Res. Dev.* **2022**, *42* (04), 133−139.
(26) Tian, Y. K.; Zhang, Z. J.; Guo, Y. H.; Wang, Z. H.; Wang, M. Study on the migration and diffusion rule of Rn in tailings stockpile under the coupling effect of temperature and pressure. *Gold* **2020**, *41* (12), 81−85.
(27) Liu, Y.; Liu, Y.; Xu, Z. H.; Hong, C. H.; Zhang, Q. C.; Yuan, J. F. Research on radon control performance of covering soil in uranium tailings reservoir under long time high temperature. *China Saf. Sci. J.* **2020**, *30* (03), 171−177, DOI: 10.16265/J.CNKI.ISSN1003-3033.2020.03.026.
(28) Wang, H.; Wang, W. H.; He, R. C.; Hong, C. H.; Wang, J.; Li, X. Y.; Liu, Y. Experimental study on unsteady radon exhalation from the overburden layer of the uranium mill tailings pond under rainfall. *Sci. Technol. Nucl. Install.* **2022**, *2022*, No. 9366056, DOI: 10.1155/2022/9366056.
(29) Liang, K. Q.; Hong, C. S.; Luo, J.; Liu, P. F.; Zhao, T. J.; Zhou, Z. F.; Zeng, Z. Q.; Liu, y. Radon attenuation characteristics of compacted soil layer for uranium mill tailings pond subjected to drying-wetting cycles. *Sci. Total Environ.* **2022**, *851*, No. 158184.
(30) Li, Y. L.; Zhang, J. Stability analysis of covering layer of a decommissioned uranium tailings pond. *China Min. Mag.* **2014**, *23* (S2), 96−98.
(31) Waugh, W. J.; Smith, G. M.; Bergman-Tabbert, D.; Metzler, D. R. Evolution of cover systems for the uranium mill tailings remedial action project, USA. *Int. J. Mine Water* **2001**, *20* (04), 190−197, DOI: 10.1007/s10230-001-8104-1.
(32) Ota, M.; Iida, T.; Yamazawa, H.; Nagara, S.; Ishimori, Y.; Sato, K.; Tokizawa, T. Suppression of radon exhalation from soil by covering with clay-mixed soil. *J. Nucl. Sci. Technol.* **2007**, *44* (05), 791−800.
(33) Xin, J. Y.; Hong, C. S.; Wei, J.; Qie, J. W.; Wang, H.; Lei, B.; Li, X. Y.; Cai, Z. Q.; Kang, Q.; Zeng, Z. W.; Liu, y. A comprehensive review of radligand-ioactive pollution treatment of uranium mill tailings. *Environ. Sci. Pollut. Res.* **2023**, *30* (46), 102104−102128.
(34) Hu, L. C.; Guo, D. P.; Li, Z. H.; Li, Y. L.; Zhang, N. Design of cover system for decommissioning of uranium mill tailings pond. *Uranium Min. Metall.* **2021**, *40* (01), 70−75.
(35) Rong, F.; Liu, A. T.; Chen, L. S. Dry-wet cycle test study of size effect on surface cracks and shear strength of expansive soil. *Int. Core J. Eng.* **2020**, *6* (11), 64−73, DOI: 10.6919/ICJE.202011_6(11).0010.
(36) Duan, H.; Liu, M. X.; Yi, J.; Zhu, Z. C.; Zhu, Q.; Zhang, H. L. Propagation and closure law of cracks in the paddy soil during drying-wetting cycle. *Res. Soil. Water Conserv.* **2020**, *27* (02), 370−376.
(37) Wang, S. J.; Yang, Z. B.; Li, X.; Luo, Z. G.; Xu, C.; Li, D. Experimental study on crack evolution and strength attenuation of expansive soil under wetting-drying cycles. *Trans. Chin. Soc. Agric. Eng.* **2021**, *37* (05), 113−122, DOI: 10.11975/j.issn.1002-6819.2021.05.013.
(38) Chen, K. S. Evolution of cracks in red clay under wetting-drying cycles and its influence on shear strength. *Hydrogeol. Eng. Geol.* **2018**, *45* (01), 89−95.
(39) Liu, G. S.; Chen, Y. G.; Zeng, X. Y.; Zhang, G. B. Effects of ambient air humidity and temperature on crack development of compacted expansive soils. *Chin. J. Geotech. Eng.* **2020**, *42* (02), 260−268, DOI: 10.11779/CJGE202002007.
(40) Jiang, F. L.; Zhang, S.; Liu, Y.; Shan, P. F.; Hong, C. S.; Lei, B.; Guo, J. T. Response characteristics of internal damage evolution and surface radon exhalation rate of radioactive rock under blasting dynamic loading. *Chin. J. Rock Mech. Eng.* **2020**, *39* (S1), 2741−2750.
(41) Zhan, D. X.; Kuang, Y. Q.; Ruan, Z. Factors impacting the regional airquality in the guangdong-hong kong-macao greater bay area: a study based on grey relational analysis. *J. Tsinghua Univ. (Sci. Technol.)* **2018**, *58* (08), 761−767, DOI: 10.16511/j.cnki.qhdxxb.2018.26.031.
(42) Yu, K.; Ouyang, N. X.; Zhang, Y. Z.; Zhou, Q.; Sheng, H.; Huang, Y. X.; Yuan, H. Study on estimation method of annual average soil temperature in soil taxonomy of hunan province. *Hunan Agric. Sci.* **2019**, No. 12, 30−37.

https://doi.org/10.1021/acsomega.4c00374
ACS Omega 2024, 9, 19295−19310